# Charge separation dynamics in a narrow band gap polymer-PbS nanocrystal blend for efficient hybrid solar cells

Piliego, Claudia; Manca, Marianna; Kroon, Renee; Yarema, Maksym; Szendrei, Krisztina; Andersson, Mats R.; Heiss, Wolfgang; Loi, Maria A.

*Published in:*
Journal of Materials Chemistry

*DOI:*
10.1039/c2jm34034h



*Publication date:*
2012

Journal of Materials Chemistry

Cite this: *J. Mater. Chem.*, 2012, **22**, 24411

www.rsc.org/materials

**PAPER**

# Charge separation dynamics in a narrow band gap polymer–PbS nanocrystal blend for efficient hybrid solar cells

**Claudia Piliego,[a] Marianna Manca,[a] Renee Kroon,[b] Maksym Yarema,[c] Krisztina Szendrei,[a] Mats R. Andersson,[b] Wolfgang Heiss[c] and Maria A. Loi*[a]**

***Received 21st June 2012, Accepted 10th August 2012***
**DOI: 10.1039/c2jm34034h**



We have demonstrated efficient hybrid solar cells based on lead sulfide (PbS) nanocrystals and a narrow band gap polymer, poly[{2,5-bis(2-hexyldecyl)-2,3,5,6-tetrahydro-3,6-dioxopyrrolo[3,4-*c*]pyrrole-1,4-diyl}-*alt*-{[2,2′-(1,4-phenylene)bis-thiophene]-5,5′-diyl}], (PDPPTPT). An opportune mixing of the two materials led to the formation of an energetically favorable bulk hetero-junction with a broad spectral response. Using a basic device structure, we reached a power conversion efficiency of ~3%, which is one of the highest values reported for this class of solar cells. Photo-physical measurements carried out on the device provided insights into the working mechanism: the comparison between the time decay of the pristine polymer and the polymer–PbS blend allows us to conclude that efficient charge transfer is taking place in this hybrid system.

## Introduction

Hybrid solar cells[1,2] based on blends of semiconducting polymers and colloidal semiconductor nanocrystals (NCs)[3] represent an emerging class of devices able to combine the advantages of the two classes of materials: the high optical absorbance of conjugated polymers and the high conductance and tunable optical band gap of nanocrystals.[4,5] Among the many semiconductor nanocrystals under investigation for photovoltaic applications (CdSe,[6,7] CdS,[8,9] CdTe,[10] PbSe[11–13]), lead sulfide (PbS) NCs[14] have emerged as one of the most promising candidates, due to their high electron mobility,[15] broad absorption and stability in air.[16,17] In particular, the synthetic control over the PbS diameter allows for precise tuning of the energy gap,[18] enabling solar energy conversion in the near-infrared (NIR).[19] This represents an advantage with respect to fully organic systems, since the synthesis of organic semiconductors with broadband near-infrared light absorption is still very challenging.[20] Therefore, devices based on blends of polymer–PbS nanoparticles have additional benefit in that light is absorbed by both components in different spectral ranges.

Despite these "theoretical advantages" of hybrids over all organic devices, to date polymer–PbS systems have underperformed with respect to competing architectures.[21–25] In order to understand the reasons for the poor performance,[26] we should take into account the criteria that have to be satisfied to obtain efficient devices based on hybrid blends.

First of all the alignment of the energy levels of the components should be suitable for dissociation of photo-generated excitons into free charges at the interface. In order to address this first criterion, Ginger *et al.*[22] selected a group of polymers with suitable HOMOs to form type-II heterojunctions when blended with PbS.[27] By using photoinduced absorption spectroscopy they were able to confirm the presence of photoinduced charge transfer between poly(2,3-didecylquinoxaline-5,8-diyl-*alt*-*N*-octyldithieno[3,2-*b*:2′,3′-*d*]pyrrole) (PDTPQx), with a HOMO of 4.61 eV, and PbS NCs (~3 nm diameter). However, the maximum efficiency measured in this system was very low (0.55%), probably due to limited charge transport between the nanocrystals.

This points out that, in order to obtain an efficient hybrid system, the dynamics of exciton dissociation and charge transport have to be faster than their recombination. In this respect a critical role is played by the ligands surrounding the NC surface. The as-prepared NCs are usually covered by long alkyl chain ligands, such as trioctylphosphine (TOPO) and oleic acid (OA), which provide controlled growth conditions and ensure solubility. These ligands are electrical insulators impeding charge transport between NCs and reducing charge separation at semiconducting polymer–NP interfaces. Therefore, in order to achieve good charge photogeneration and efficient charge transport it is necessary to replace the long ligands with shorter ones.

The effect of a "post-deposition treatment" on PDTPQx-HD–PbS blend films using ethanedithiol (EDT) was studied in a recent publication.[28] By comparing samples with and without treatment, the authors found significant differences in both

[a]*Zernike Institute for Advanced Materials, University of Groningen, Nijenborgh 4, 9747 AG Groningen, The Netherlands. E-mail: m.a.loi@rug.nl*
[b]*Polymer Technology, Department of Chemical and Biological Engineering, Chalmers University of Technology, Göteborg, Sweden*
[c]*Institute for Semiconductor and Solid State Physics, University of Linz, Linz, Austria*

polaron lifetime and device performance, suggesting the presence of electronic wave function overlaps. The effect of the post-deposition treatment is therefore an increased mobility and decreased recombination loss, as shown in PbS solar cells.[29]

Finally, the morphology of the hybrid composite has to provide a high interface area for exciton dissociation and simultaneously a continuous transport pathway for each charge to their respective electrodes. This is particularly challenging to achieve, since often ligand exchange treatments result in a more coarse morphology and higher surface roughness.[30]

The stringent requirements for the realization of efficient hybrid blends have limited the performance of the PbS–polymer system until now. Only very recently Prasad's group[31] showed that it is possible to meet all these criteria and to achieve high efficiency in hybrid devices based on PbS NCs. By selecting a suitable narrow band-gap polymer, poly(2,6-(*N*-(1-octylnonyl) dithieno[3,2-*b*:20,30-*d*]pyrrole)-*alt*-4,7-(2,1,3-benzothiadiazole)) (PDTPBT),[32] and performing a post-deposition ligand exchange, they obtained an energetically favorable hetero-junction with a broad spectral response and power conversion efficiency over 2%. The authors showed the importance of the energy level matching between the polymer and the nanoparticles and the efficacy of the post-deposition ligand exchange treatment. However, they did not explore the carrier generation dynamics or examine charge transfer at the polymer–PbS interface. Therefore, there is still a lack of fundamental understanding of the interactions between the polymer and the nanocrystals.

In this paper we aim to shed light on the working principle of a hybrid PbS–polymer system: after presenting the device performance, we explore the charge separation dynamics and we compare the results with those obtained for the polymer–fullerene blend. The bulk hetero-junction solar cells based on PbS NCs and a narrow band gap polymer, PDPPTPT (poly[{2,5-bis(2-hexyldecyl)-2,3,5,6-tetrahydro-3,6-dioxopyrrolo[3,4-*c*]pyrrole-1,4-diyl}-*alt*-{[2,2′-(1,4-phenylene)bisthiophene]-5,5′-diyl}]),[33] showed an efficiency of 2.9% (see Table 1). Most of the previous spectroscopic studies on PbS hybrid blends have been carried out on a thin film and not on the actual device, making it difficult to correlate the spectroscopic evidence directly to the efficiency. Here instead we performed the optical measurements directly on the devices, which provided us the opportunity to draw some exhaustive conclusions on the working principle of this efficient hybrid system.

## Experimental

### Materials

**Synthesis of PbS NCs.** Lead(II) oxide (99.999%), hexamethyldisilathiane (HMDT, purum grade), oleic acid (OA, 90%), octadecene (ODE, 90%, techn.), toluene (≥99.9%), hexane (≥97%) and ethanol (99.8%) were purchased from Sigma-Aldrich. The synthesis of uniform PbS NCs was performed *via* a modified method of Hines and Scholes using a standard airless Schlenk line technique.[34] Briefly, ODE (93.75 ml), PbO (2.25 g), and OA (6.25 ml) were loaded into a 250 ml three-neck flask. The reagents were purified under vacuum at 150 °C for 90 minutes, and then kept at 150 °C under an argon flow for 30 minutes. During this time, lead(II) oleate was formed *in situ*, as indicated by the discoloration of the reaction mixture. HMDT (1.05 ml) was dissolved in ODE (50 ml) in a glove box, and swiftly added to the reaction mixture at 150 °C. The color of reaction mixture changed to deep brown, indicating the fast formation of PbS NCs. Next, the PbS NC solution was cooled to $T = 100$ °C and annealed at this temperature for about 5 minutes. Finally, the reaction mixture was quenched with a water bath. For the purification of PbS NCs, the washing procedure was performed with subsequent additions of hexane and ethanol, followed by centrifugation (6000*g*). The hexane–ethanol washing cycle was repeated 3 times. At the end of the purification procedure the PbS NCs were dissolved in toluene, forming a long-term stable colloid. The yield of PbS NCs was about 75%. The PbS NCs were subsequently dried and re-dissolved in chloroform for device fabrication.

**Synthesis of PDPPTPT.** Polymerization of (poly[{2,5-bis(2-hexyldecyl)-2,3,5,6-tetrahydro-3,6-dioxopyrrolo[3,4-*c*]pyrrole-1,4-diyl}-*alt*-{[2,2′-(1,4-phenylene)bisthiophene]-5,5′-diyl}]) PDPPTPT was conducted as reported by Bijleveld *et al.*,[33] under slightly modified experimental conditions. 1,4-Bis(4,4,5,5-tetramethyl-1,3,2-dioxaborolan-2-yl)benzene was obtained from Sigma Aldrich and recrystallized from EtOH prior to use. 3,6-Bis(5-bromothiophen-2-yl)-2,5-bis(2-hexyldecyl)pyrrolo[3,4-*c*] pyrrole-1,4(2*H*,5*H*)-dione was kindly donated by BASF and used as received. PDPPTPT was obtained as dark purple fibers (96%). $M_n$: 15 kg mol$^{-1}$, $M_w$: 23 kg mol$^{-1}$, PDI: 1.5. From the square wave voltammetry measurements: $E_{red,onset}$: −1.46 V and $E_{ox,onset}$: 0.48 V.

The molecular weights were calculated according to relative calibration with polystyrene standards. Square-wave voltammetry (SWV) measurements were carried out on a CH-Instruments 650A Electrochemical Workstation.

### Device fabrication

After the optimization of the percentage of polymer in the nanocrystal blend, the best results were obtained with PDPPTPT:PbS 10 : 90 wt%. The blend of PDPPTPT:PbS–OA (10 : 90 wt%) in chloroform (5 mg ml$^{-1}$) was kept overnight stirring at 50 °C to obtain a good mixing. The blend was then spin-coated on a pre-cleaned patterned ITO substrate at 4000 rpm for 60 seconds to form a layer of ~8 nm. A solution of 1,4-benzenedithiol (BDT) in acetonitrile (0.02 M) was then deposited on top of the layer to replace the native ligand. After soaking the layer for 30 seconds, the substrate was spun at 4000 rpm for 1

**Table 1** Average photovoltaic performance values. (Values in the brackets are the best values recorded)

| Active layer | $V_{OC}$ (V) | $J_{SC}$ (mA cm$^{-2}$) | FF (%) | PCE (%) |
|---|---|---|---|---|
| PDPPTPT:PbS (10 : 90 wt%) | 0.46 (0.47) | −11 (−12.5) | 45 (49) | 2.3 (2.9) |
| PDPPTPT:$PC_{61}BM$ (1 : 2) | 0.72 (0.74) | −5.7 (−6.3) | 49 (52) | 2.0 (2.4) |

 

minute to remove the solvent. These steps were repeated several times (15–18 layers) until the desired thickness (110–120 nm) was reached. The PDPPTPT:$PC_{61}BM$ 1 : 2 blend in chloroform (22 mg $ml^{-1}$) was deposited on top of a PEDOT:PSS layer (~40 nm) by spin-coating. The devices with an active area of 4 $mm^2$ were completed by thermal evaporation of the cathode consisting of 1 nm LiF and 100 nm Al. Several devices were fabricated in order to optimise the thickness and the ratio between the two components of the blends. The average and best performance values are reported in Table 1.

### Measurements

Current–voltage characteristics were recorded using a Keithley 2400 Source Meter with the device kept in a nitrogen filled glove box. Measurements were performed in the dark and under illumination from a Steuernagel Solar Constant 1200 metal halide lamp calibrated to 1 sun intensity and corrected for spectral mismatch with the AM 1.5G spectrum using a Si reference cell. Contribution to the photocurrent from regions outside the anode–cathode overlap area was eliminated using a mask with a slightly smaller aperture than the device area. Incident photon-current conversion efficiency (IPCE) spectra were measured from 400 nm to 1400 nm using a custom-built set-up consisting of a 50 W quartz tungsten halogen lamp (Newport research series) with a highly stable radiometric power supply, 33 narrow band-pass filters (CVI laser), a trans-impedance amplifier and a Stanford Research System SR830 lock-in amplifier. The spectral response was measured relative to that of a calibrated Si (Newport 818-SL) and a Ge (Oriel 71653) photodiode.

Layer thickness measurements were performed using a Veeco Dektak 6M profilometer. Absorption spectra were recorded using a Perkin Elmer lambda 900 spectrometer.

Atomic force microscopy (AFM) images of the PDPPTPT:PbS layer after the BDT treatment were recorded with a Multimode AFM nanoscope IV Scanning Probe Microscope Controller functioning in tapping mode.

Steady-state and time resolved PL measurements were performed on the devices. For the pristine polymer the layer was spin-coated on glass substrates following the same procedure. The samples were prepared in inert nitrogen atmosphere and encapsulated to protect them from air during the measurements. The samples were excited with a Ti:sapphire laser delivering pulses of about 150 fs width at approximately 730 nm. The steady-state PL spectra in the near-infrared were obtained with an InGaAs detector from Andor. The PL spectra were corrected for the spectral response of the set-up using a calibrated light source. Time-resolved traces were recorded with a NIR sensitive Hamamatsu streak camera working in synchroscan mode.

## Results and discussion

Fig. 1 shows the absorption spectrum and the molecular structure of PDPPTPT: this polymer when used as an electron donor in combination with $PC_{61}BM$ has shown good power conversion efficiency (PCE), after optimization of the device morphology with an additive.[33] The absorption spectrum of the PbS NCs dispersed in toluene is shown in Fig. 1b: the as-prepared PbS NCs, capped with the OA ligand to provide good dispersibility,

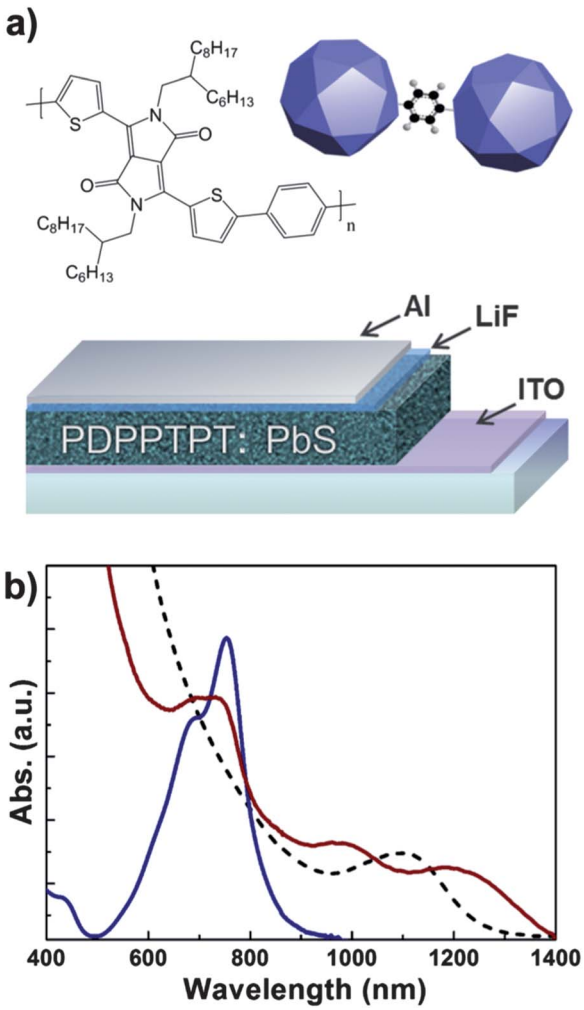


**Fig. 1** (a) Molecular structure of the PDPPTPT polymer, schematic of the BDT crosslinked PbS nanocrystals and of the device structure. (b) Absorption spectra of the PDPPTPT film (blue line), OA-capped PbS nanocrystals dispersed in toluene (dashed black line) and of the PDPPTPT:PbS (10 : 90 wt%) blend film (red line) after the BDT ligand exchange treatment.

display the first excitonic peak around 1100 nm. Fig. 1b also shows the absorbance spectrum of the PDPPTPT:PbS blend film with a 10 : 90 weight ratio after the post-deposition treatment. The short bi-dentate ligands, such as BDT, effectively replace the long insulating chains, reducing the inter particle spacing. This leads to the crosslinking of the thin layer and to an increase of the electronic coupling between NCs.[35] The absorption spectrum of the blend after the ligand exchange treatment is shown in Fig. 1b: the contribution from the polymer is visible in the range of 600–800 nm together with the absorption of the NCs in the NIR region. In particular, the contribution to the absorption of the PbS NCs in the thin film after ligand exchange appears red-shifted and broadened compared to the absorption in solution. This is a result of the cross-linking process and it has been attributed to the wave function overlaps and to the appearance of defect states.[36] Similar features have also been observed for nanocrystals treated with 1,2-ethanedithiol (EDT);[37,38] instead usually no red-shift can be observed in the absorption spectra of the PbS–OA film compared to PbS–OA solution.[39]

Hybrid solar cells were fabricated, using a simple device structure, as shown in Fig. 1a. A thin layer of PDPPTPT:PbS–OA (10 : 90 wt%) blend was deposited on top of the ITO substrate by spin-coating, followed by the ligand exchange treatment. The PDPPTPT:PbS blend layer is stable against the chemical treatment: the PDPPTPT polymer is not dissolved while the OA ligands on the surface of the NCs are selectively exchanged with the BDT molecules. The exchange reaction performed with BDT is milder than with EDT, leaving a smoother layer after the treatment. This allowed us to obtain a uniform and crack-free hybrid film without macroscopic phase segregation, as shown by the atomic force microscopy images in Fig. 2. By considering the ratio between the two components, PDPPTPT:PbS (10 : 90 wt%), we assume that small domains of polymer are trapped in the NC matrix. This allows for a large contact area between the two materials which is beneficial for the exciton dissociation. In addition to the formation of a favorable hetero-junction morphology between the polymer and the nanocrystals, the relative position of their energy levels (inset in Fig. 3b)[27,33] is suitable for exciton separation and carrier extraction. Therefore the combination of the PbS nanoparticles with this narrow band gap polymer is expected to provide good photovoltaic performance.

Fig. 3a shows the $J$–$V$ characteristic of the best PDPPTPT:PbS blend device measured under AM 1.5 illumination at 100 mW cm$^{-2}$. The device exhibits a $J_{sc}$ of 12.5 mA cm$^{-2}$, $V_{oc}$ of 0.47 V, and a FF of 49%, resulting in an overall PCE of 2.9%. This is the highest efficiency reported to date for hybrids using a simple device structure, without additional interlayers at the interface with the electrodes. It has been shown that the insertion of a thin hole blocking buffer layer, such as $TiO_2$ [29,33] or ZnO,[40] on top of the active layer can dramatically improve the performance. Fig. 3b compares the Incident Photon-Current Conversion Efficiency (IPCE) spectrum of the device fabricated with the PDPPTPT:PbS blend and the absorption spectrum of the same active layer. The IPCE spectrum obtained from the device is consistent with the film absorption spectrum showing the combined contribution to the photocurrent of PDPPTPT and PbS. This proves that blending the narrow band gap polymer and the NIR absorbing PbS NCs gives rise to a broad response, from the UV to the NIR spectral range.

To gain more insight into the photovoltaic performance and physical processes in the hybrid blend, we carried out steady state and time resolved photoluminescence measurements on the solar cell. The basic structure used for the device allowed us to carry out the spectroscopic measurements directly on the device and to compare the results to analogous measurements performed on the PDPPTPT:$PC_{61}BM$ blend, here used as a reference system. Using pure chloroform for processing the blend, the polymer in the optimized weight ratio of 1 : 2 with $PC_{61}BM$ shows only modest PCEs of 2.45%, due to low photocurrent (see Table 1). These results are in agreement with previous reports[33] where it has been shown that the efficiency in these devices is mainly limited by the de-mixing of the polymer:fullerene blend. The morphology of this fully organic blend can be greatly improved by adding a high boiling point solvent during the processing, leading to much higher PCE.[33]

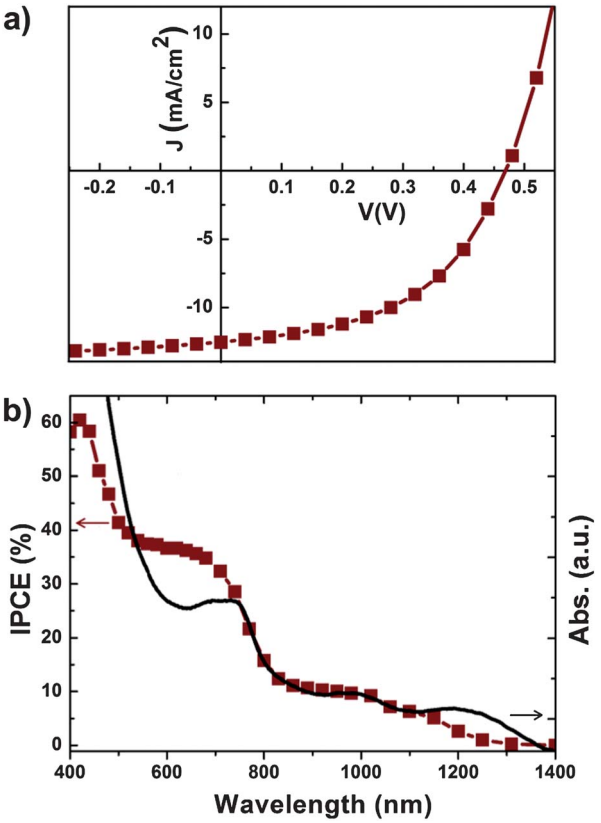


**Fig. 3** (a) $J$–$V$ characteristic of the PDPPTPT:PbS (10 : 90 wt%) blend device under AM 1.5G (100 mW cm$^{-2}$) illumination. (b) Plots of the IPCE of the blend device (red square) and the absorption spectrum (black line) of the BDT-treated blend film.

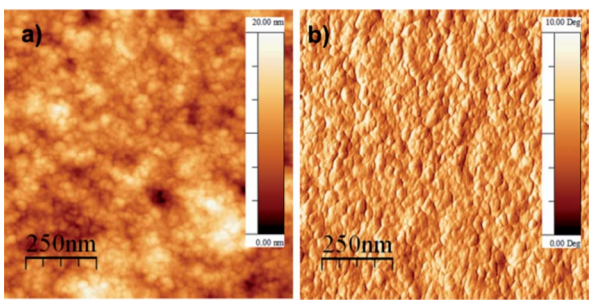


**Fig. 2** Atomic force microscopy images in tapping mode: (a) surface morphology and (b) phase of the PDPPTPT:PbS (10 : 90 wt%) blend after the BDT treatment, the scan area is 1 × 1 μm, RMS roughness 2.7 nm.

The normalized PL spectra collected upon excitation at 730 nm of PDPPTPT, PDPPTPT:$PC_{61}BM$ (1 : 2), and PDPPTPT:PbS (10 : 90 wt%) films are shown in Fig. 4a.

The PL of PDPPTPT is characterized by a unique band centered at ~907 nm, with a full width at half-maximum (FWHM) of ~217 nm.

From transient measurements we extracted the lifetime of excitons in the PDPPTPT polymer. The film displays a mono exponential decay with a time constant of about 35 ps. This lifetime appears to be much shorter than the average lifetime of conjugated polymers; however, it is typical of efficient narrow band-gap polymers. For comparison, a PL decay-time of 65 ps

 

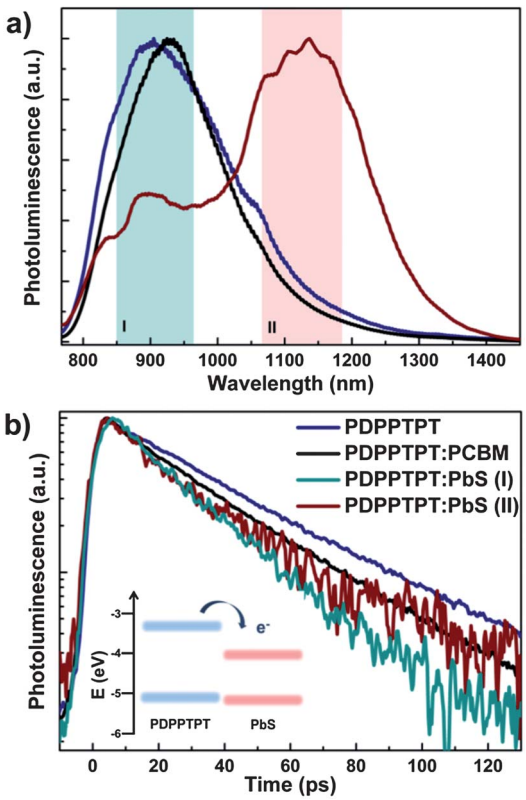


**Fig. 4** (a) Normalized photoluminescence spectra of PDPPTPT, PDPPTPT:$PC_{61}BM$ (1 : 2) and PDPPTPT:PbS (10 : 90 wt%) films excited at 730 nm and (b) dynamics of PDPPTPT, PDPPTPT:$PC_{61}BM$ (1 : 2) and PDPPTPT:PbS (10 : 90 wt%). Panels (I) and (II) indicate the wavelength range over which the dynamic traces are integrated. Inset: approximate energy level diagram of PDPPTPT and PbS (the levels of the polymer are calculated from cyclic voltammetry and the levels of the nanocrystals are from ref. 27).

was observed in poly[(4,40-bis(2-ethylhexyl)dithieno[3,2-*b*:20,30-*d*]silole)-2,6-diyl-*alt*-(4,7-bis(2-thienyl)-2,1,3-benzothiadiazole)-5,50-diyl] (Si–PCPDTBT), one of the most efficient narrow band-gap polymers reported.[41]

To understand the dynamics in the hybrid system we compared the behaviors of the two blends: polymer–fullerene and polymer–PbS. The normalized PL spectrum of the PDPPTPT:$PC_{61}BM$ blend is red-shifted by ~20 nm with respect to the pristine polymer film. This spectrum can also be described by a unique band with the maximum at ~927 nm and a FWHM of ~180 nm.

The PL spectrum of the PDPPTPT:PbS blend instead shows the appearance of a second emission peak at a wavelength around 1150 nm, which is the emission of the NCs.[36] Due to the different thicknesses of the PDPPTPT:$PC_{61}BM$ and PDPPTPT:PbS films, a direct comparison of the PL intensities and an estimation of the PL quenching in the two blends with respect to the PL of the pristine polymer is not possible. The observation of PL quenching would be the proof that the predominant process is charge transfer between the two components in the blend and that no energy transfer is taking place.

This obstacle is overcome by studying the dynamics of the PL (Fig. 4b). Fast PL decay times are in fact the optical signatures of short-lived excited states and an indication of the rapid charge transfer between the two components in the blend.[42] Therefore we measured the PL decays in the two blends. (Note that the time resolution of the experimental set-up in the configuration used for these measurements is ~3 ps.)

The PL decay of the PDPPTPT:$PC_{61}BM$ blend was detected at ~900 nm, to be mono exponential with a time constant of about 28 ps.

The PL decays of the PDPPTPT:PbS blend were detected in two different ranges: at ~900 nm (range I), corresponding to the maximum PL intensity of the neat polymer, and at ~1150 nm (range II), corresponding to the maximum PL intensity of the peak associated with the PbS-NC emission (Fig. 4a). The PL decay of the higher energy peak (range I) is bi-exponential with a very fast initial decay component (10 ps) and a tail of about 25 ps. Likewise, the lower energy part of the emission (range II) shows an initial fast decay of about 18 ps and a longer tail of about 68 ps. The fast decay time, detected in range II, could be a residue of the emission of the polymer, while the long tail is the signature of the NC decay. In the hybrid film the decay time of the NCs is reduced by more than three orders of magnitude with respect to the neat PbS film: the PL lifetime of the same PbS NCs, deposited with the same procedure, is ~200 ns.[43]

These measurements show that in both blends the decay times are lower than the one detected in the pristine polymer, suggesting that efficient charge transfer is taking place in the two systems.

Moreover, in the hybrid thin films excited states are created both in the polymer and in the PbS NCs, as shown by the optical measurements and by the IPCE spectrum. After excitation, efficient transfer of electrons from the PDPPTPT polymer to the PbS nanoparticles is taking place. Even if the offset of the HOMO levels (inset in Fig. 4b) is limited with respect to the LUMO level difference, excitation in the nanocrystals still results in the transfer of holes from the nanocrystals to the polymer. (Note that the relative position of the energy levels is only indicative, since an exact estimation of the HOMO/LUMO values of the polymer and the PbS nanocrystals in the blend is not available). A similar mechanism has been observed in hybrid ternary blends based on PbS nanocrystals.[43,44]

Regarding the causes limiting the performance, the dominant mechanisms are different in the two systems. In the polymer–$PC_{61}BM$ sample the main factor is probably the charge recombination of the initially charge separated states, due to the non-optimized morphology. This has been previously proposed by comparing the intensity of the triplet absorption in the PIA signal of the pristine polymer and the blend.[33]

In the polymer–PbS film, the recombination processes of the charge separated states can be ascribed to the presence of defects at the nanocrystal–polymer interface and traps, probably located on the nanocrystal surface.[36] The performance can therefore be improved by optimizing the ligand exchange process in order to limit the formation of defects and traps.

Finally the carrier mobility of the single component in the blend is a critical factor for the efficient transport of the dissociated charges to the electrodes. Both the PDPPTPT polymer[33] and the PbS nanocrystals[45] have shown ambipolar behavior in field effect transistor measurements, so we can assume that electrons and holes can travel through the interpenetrating network composed of the two materials. To better investigate this point, studies on

the transport properties of nanocrystals and the hybrid blend are in progress and they will be reported in the future.

## Conclusions

In conclusion, we reported the fabrication of an efficient hybrid bulk hetero-junction photovoltaic device containing a narrow-bandgap polymer (PDPPTPT) and NIR absorbing PbS NCs. An opportune mixing of the two materials led to the formation of an energetically favorable hetero-junction with a broad spectral response and a PCE of ~3%. PL lifetime measurements of the polymer–PbS and polymer–$PC_{61}BM$ blends were performed to gain a deeper understanding of the charge transfer mechanisms. Our results show that the charge separation efficiency is the same in the fully organic and the hybrid blends and that performances are in part limited by the morphology control and the presence of traps. However, other factors are critical and they need to be investigated; for example, the impact of the large variation in dielectric constant between the polymer ($\varepsilon \sim 2.5$ to 3)[46] and the nanocrystal phase ($\varepsilon \sim 17$)[47] and the influence of the intrinsic difference in mobility of the two components.

We believe that our work can inspire a renewed interest in the solution processable hybrid systems. If the processing issues can be addressed, taking into account the large variety of narrow band gap polymers and tunable nanoparticles available, this technology can potentially match and even overcome the performance of all organic blends.

## Acknowledgements

Financial support from the Zernike Institute for Advanced Materials, the FOM Focus Group Groningen and the Austrian Science Fund FWF (project IR_ON F2505) is gratefully acknowledged. BASF is acknowledged for kindly providing the monomer for the synthesis of the PDPPTPT polymer. The authors thank J. Harkema, F. van der Horst and A. Kamp for technical support.

## Notes and references

1 T. Xu and Q. Qiao, *Energy Environ. Sci.*, 2011, **4**, 2700.
2 Y. Zhou, M. Eck and M. Krüger, *Energy Environ. Sci.*, 2010, **3**, 1851.
3 D. V. Talapin, J.-S. Lee, M. V. Kovalenko and E. V. Shevchenko, *Chem. Rev.*, 2010, **110**, 389.
4 R. Debnath, O. Bakr and E. H. Sargent, *Energy Environ. Sci.*, 2011, **4**, 4870.
5 P. Reiss, E. Couderc, J. De Girolamo and A. Pron, *Nanoscale*, 2011, **3**, 446.
6 N. Yaacobi-Gross, M. Soreni-Harari, M. Zimin, S. Kababya, A. Schmidt and N. Tessler, *Nat. Mater.*, 2011, **10**, 974.
7 J. N. de Freitas, I. R. Grova, L. C. Akcelrud, E. Arici, N. S. Sariciftci and A. F. Nogueira, *J. Mater. Chem.*, 2010, **20**, 4845.
8 L. X. Reynolds, T. Lutz, S. Dowland, A. MacLachlan, S. King and S. A. Haque, *Nanoscale*, 2012, **4**, 1561.
9 H. C. Leventis, S. P. King, A. Sudlow, M. S. Hill, K. C. Molloy and S. A. Haque, *Nano Lett.*, 2010, **10**, 1253.
10 W. Yu, H. Zhang, Z. Fan, J. Zhang, H. Wei, D. Zhou, B. Xu, F. Li, W. Tian and B. Yang, *Energy Environ. Sci.*, 2011, **4**, 2831.
11 C. Y. Kuo, M. S. Su, Y. C. Hsu, H. N. Lin and K. H. Wei, *Adv. Funct. Mater.*, 2010, **20**, 3555.
12 W. L. Ma, S. L. Swisher, T. Ewers, J. Engel, V. E. Ferry, H. A. Atwater and A. P. Alivisatos, *ACS Nano*, 2011, **5**, 8140.
13 K. M. Noone, N. C. Anderson, N. E. Horwitz, A. M. Munro, A. P. Kulkarni and D. S. Ginger, *ACS Nano*, 2009, **3**, 1345.
14 H. Fu and S.-W. Tsang, *Nanoscale*, 2012, **4**, 2187.
15 J.-S. Lee, M. V. Kovalenko, J. Huang, D. S. Chung and D. V. Talapin, *Nat. Nanotechnol.*, 2011, **6**, 348.
16 J. Tang, K. W. Kemp, S. Hoogland, K. S. Jeong, H. Liu, L. Levina, M. Furukawa, X. Wang, R. Debnath, D. Cha, K. W. Chou, A. Fischer, A. Amassian, J. B. Asbury and E. H. Sargent, *Nat. Mater.*, 2011, **10**, 765.
17 M. Sykora, A. Y. Koposov, J. A. McGuire, R. K. Schulze, O. Tretiak, J. M. Pietryga and V. I. Klimov, *ACS Nano*, 2010, **4**, 2021.
18 F. W. Wise, *Acc. Chem. Res.*, 2000, **33**, 773.
19 J. Tang and E. H. Sarget, *Adv. Mater.*, 2011, **23**, 12.
20 A. Facchetti, *Chem. Mater.*, 2011, **23**, 733.
21 A. Guchhait, A. K. Rath and A. J. Pal, *Appl. Phys. Lett.*, 2010, **96**, 073505.
22 K. M. Noone, E. Strein, N. C. Anderson, P.-T. Wu, S. A. Jenekhe and D. S. Ginger, *Nano Lett.*, 2010, **10**, 2635.
23 J. Seo, S. J. Kim, W. J. Kim, R. Singh, M. Samoc, A. N. Cartwright and P. N. Prasad, *Nanotechnology*, 2009, **20**, 6.
24 Z. Wang, S. Qu, X. Zeng, C. Zhang, M. Shi, F. Tan, Z. Wang, J. Liu, Y. Hou, F. Teng and Z. Feng, *Polymer*, 2008, **49**, 4647.
25 A. R. Watt, D. Blake, J. H. Warner, E. A. Thomsen, E. L. Tavenner, H. Rubinsztein-Dunlop and P. Meredith, *J. Phys. D: Appl. Phys.*, 2005, **38**, 2006.
26 H. Borchert, *Energy Environ. Sci.*, 2010, **3**, 1682.
27 B.-R. Hyun, Y.-W. Zhong, A. C. Bartnik, L. Sun, H. D. Abruña, F. W. Wise, J. D. Goodreau, J. R. Matthews, T. M. Leslie and N. F. Borrelli, *ACS Nano*, 2008, **2**, 2206.
28 K. M. Noone, S. Subramaniyan, Q. Zhang, G. Cao, S. A. Jenekhe and D. S. Ginger, *J. Phys. Chem. C*, 2011, **115**, 24403.
29 D. A. R. Barkhouse, A. G. Pattantyus-Abraham, L. Levina and E. H. Sargent, *ACS Nano*, 2008, **2**, 2356.
30 A. J. Moulé, L. Chang, C. Thambidurai, R. Vidu and P. Stroeve, *J. Mater. Chem.*, 2012, **22**, 2351.
31 J. Seo, M. J. Cho, D. Lee, A. N. Cartwright and P. N. Prasad, *Adv. Mater.*, 2011, **23**, 3984.
32 W. Yue, Y. Zhao, S. Shao, H. Tian, Z. Xie, Y. Geng and F. Wang, *J. Mater. Chem.*, 2009, **19**, 2199.
33 J. C. Bijleveld, V. S. Gevaerts, D. Di Nuzzo, M. Turbiez, S. G. J. Mathijssen, D. M. de Leeuw, M. M. Wienk and R. A. J. Janssen, *Adv. Mater.*, 2010, **22**, E242.
34 M. Hines and G. Scholes, *Adv. Mater.*, 2003, **15**, 1844.
35 K. Szendrei, W. Gomulya, M. Yarema, W. Heiss and M. A. Loi, *Appl. Phys. Lett.*, 2010, **97**, 203501.
36 K. Szendrei, M. Speirs, W. Gomulya, D. Jarzab, M. Manca, O. V. Mikhnenko, M. Yarema, B. J. Kooi, W. Heiss and M. A. Loi, *Adv. Funct. Mater.*, 2012, **22**, 1598.
37 J. M. Luther, M. Law, M. C. Beard, Q. Song, M. O. Reese, R. J. Ellingson and A. J. Nozik, *Nano Lett.*, 2008, **8**, 3488.
38 J. Tang, L. Brzozowski, D. A. R. Barkhouse, X. Wang, R. Debnath, R. Wolowiec, E. Palmiano, L. Levina, A. G. Pattantyus-Abraham, D. Jamakosmanovic and E. H. Sargent, *ACS Nano*, 2010, **4**, 869.
39 J. J. Choi, J. Luria, B.-R. Hyun, A. C. Bartnik, L. Sun, Y.-F. Lim, J. A. Marohn, F. W. Wise and T. Hanrath, *Nano Lett.*, 2010, **10**, 1805.
40 W. Yu, H. Zhang, Z. Fan, J. Zhang, H. Wei, D. Zhou, B. Xu, F. Li, W. Tian and B. Yang, *Energy Environ. Sci.*, 2011, **4**, 2831.
41 M. C. Scharber, M. Koppe, J. Gao, F. Cordella, M. A. Loi, P. Denk, M. Morana, H.-J. Egelhaaf, K. Forberich, G. Dennler, R. Gaudiana, D. Waller, Z. Zhu, X. Shi and C. J. Brabec, *Adv. Mater.*, 2010, **22**, 367.
42 O. V. Mikhnenko, H. Azimi, M. Scharber, M. Morana, P. W. M. Blom and M. A. Loi, *Energy Environ. Sci.*, 2012, **5**, 6960.
43 D. Jarzab, K. Szendrei, M. Yarema, S. Pichler, W. Heiss and M. A. Loi, *Adv. Funct. Mater.*, 2011, **21**, 1988.
44 G. Itskos, A. Othonos, T. Rauch, S. F. Tedde, O. Hayden, M. V. Kovalenko, W. Heiss and S. A. Choulis, *Adv. Energy Mater.*, 2011, **1**, 802.
45 W.-K. Koh, S. R. Saudari, A. T. Fafarman, C. R. Kagan and C. B. Murray, *Nano Lett.*, 2011, **11**, 4764.
46 M. A. Loi, S. Toffanin, M. Muccini, M. Forster, U. Scherf and M. Scharber, *Adv. Funct. Mater.*, 2007, **17**, 2111.
47 K. Szendrei, F. Cordella, M. V. Kovalenko, M. Boberl, G. Hesser, M. Yarema, D. Jarzab, O. V. Mikhnenko, A. Gocalinska, M. Saba, F. Quochi, A. Mura, G. Bongiovanni, P. W. M. Blom, W. Heiss and M. A. Loi, *Adv. Mater.*, 2009, **21**, 683.

 